# NUMERICAL SIMULATION OF THE FLOW FIELD STRUCTURE OF LIQUID NITROGEN JET

by

***Chengzheng CAI*** [a, b, *]***, Keda REN*** [a, b]***, Qinghua LI*** [a, b]***,***

[a] State Key Laboratory for GeoMechanics and Deep Underground Engineering, China University of Mining and Technology, Xuzhou 221116, China
[b] School of Mechanics and Civil Engineering, China University of Mining and Technology, Xuzhou 221116, China

*Liquid nitrogen jet (LNJ) is regarded as an excellent technology for the well drilling and reservoir fracturing. To evaluate the flow field structure of LNJ, a two-dimensional computation fluid dynamic model is established. The transient velocity and temperature fields of LNJ is simulated. The results show that the LNJ also clearly presented the velocity boundary and potential core region similar to the water jet. Given the temperature difference between the jet and surrounding fluid, the LNJ has an obvious temperature boundary, on which the jet temperature is equal to the initial value. According to the phase of the jet, the flow structure can be divided into the LNJ and non-LNJ regions. The temperature boundary shows a larger width than the velocity boundary for LNJ. Moreover, both width and length of the LNJ region are greater than the potential core region.*

Key words*: Liquid nitrogen jet, Flow field structure, Well drilling, Reservoir fracturing, Numerical simulation*

## Introduction

In past decades, the high-pressure water jet has played the significant roles in the petroleum engineering [1]. However, with the increasing attention turned toward unconventional resources, the new requirements are proposed. First, the work fluid, which is used to develop these reservoirs, should have an important role in inhibiting the clay swelling and water blocking damage [2]. Second, the pollution on the underground and surface water resources should be avoided as much as possible [3]. Third, in the arid areas, the water consumed should be reduced to the greatest extent [4]. In light of the above issues, a novel jet technology — liquid nitrogen jet (LNJ) was proposed in [5].

As the LNJ is involved in non-water fluid, the issues of the water pollution and consumption are solved perfectly. Above all, the temperature of the liquid nitrogen is

[*] Corresponding author. E-mail: caicz@cumt.edu.cn

extremely low and it can generate the great thermal stress on the surface of materials [6]. Thus, the rock breaking and cracking capabilities will be enhanced significantly if the LNJ is used in the drilling or fracturing processes. Many previous investigations indicated that LNJ has stronger impact capability and better coal breaking performance than water jet because liquid nitrogen cooling can generate additional cracking effect on rock [7-10]

The LNJ involves the heat transfer and the change in fluid properties. Thus, its flow field and jet structure will become more complex than those of the water jet will. In this work, a two-dimensional CFD model will be built to simulate the velocity and temperature distributions.

## The model proposed

### *The geometric model and boundary conditions*

A nozzle with an axisymmetric structure was employed to generate the LNJ. Thus, only a two-dimensional model (Fig. 1) was built to analyze the flow field structure of LNJ. The geometric model is consisted of the fluid (green region) and solid (red region) parts. As this model was symmetric, only the half-flow domain was presented. To eliminate the effect of the wall boundary on the flow field of the LNJ maximally, the axial distance from the nozzle outlet to the right wall was set to 570 mm, and the radial distance from the axis to the top wall was set to 270 mm. The thickness of the solid part was 30 mm. The inlet of the nozzle and the outlet of the flow domain were set as the pressure–inlet and pressure–outlet boundary conditions, respectively. The fluid–solid interfaces (shown in Fig. 1) were designated as the conjugated boundary conditions, while the other walls were the non-slip wall boundary conditions. The axes of the fluid and solid parts were set as the axial symmetry boundary conditions.

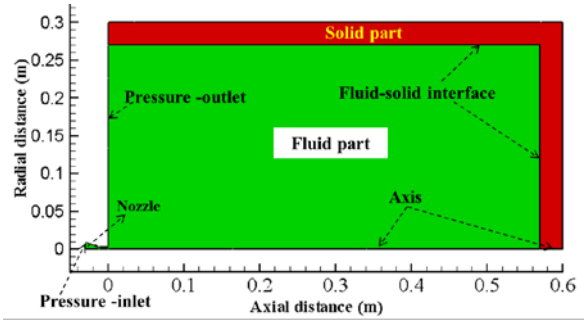


Fig. 1. The shematic of the geometric model for the LNJ flow field.

### *The mathematical model*

In this model, the flow equations (mass conservation, momentum, and energy equations) and heat transfer equations should be solved in a coupled manner to obtain the velocity, pressure, and temperature distributions of the LNJ [10]. The k-ε model was used to solve the turbulent flow field. As the LNJ involved high-pressure and low-temperature flow, real gas models instead of the ideal-gas models were adopted to calculate the properties of

nitrogen. To improve the accuracy of numerical simulation, the models of the National Institute of Standards and Technology (NIST) were used. Four properties of nitrogen were involved during the simulation were presented as follows: density, isobaric heat capacity, viscosity, and thermal conductivity.

The density and isobaric heat capacity were calculated in [11]. The Helmholtz energy ($a$) is the function of density ($\rho$) and temperature ($T$), while the reduced Helmholtz energy is the function of reduced density ($\delta$) and reduced temperature ($\tau$), e.g.,

$$\alpha(\delta,\tau) = a(\rho,T)/(RT) = \alpha^o(\delta,\tau) + \alpha^r(\delta,\tau) \tag{1}$$

where $\alpha(\rho,T)$ is the Helmholtz energy, $\alpha(\delta,\tau)$ is the reduced Helmholtz energy, $\alpha(\delta,\tau)$ is the ideal gas component, and $\alpha^r(\delta,\tau)$ is the residual part of the reduced Helmholtz energy, $R = 0.2968$, $\delta=\rho/\rho_c$, $\tau = T_c/T$, $\rho$ is the density, $\rho_c$ is the critical density, $T$ is the temperature, and $T_c$ is the critical temperature.

The density and isobaric heat capability of nitrogen were evaluated by [11]

$$p(\delta,\tau) = \rho RT\left(1 + \delta\left(\frac{\partial \alpha^r}{\partial \delta}\right)_\tau\right) \tag{2}$$

$$\frac{C_P(\delta,\tau)}{R} = -\tau^2(\alpha^o_{\tau\tau} + \alpha^r_{\tau\tau}) + \frac{(1 + \delta\alpha^r_\delta - \delta\tau\alpha^r_{\delta\tau})^2}{1 + 2\delta\alpha^r_\delta + \delta^2\alpha^r_{\delta\delta}} \tag{3}$$

where $p$ is the pressure.

The Lemmon and Jacobsen models were used to calculate the viscosity and thermal conductivity, given as [12]:

$$\mu(\rho,T) = \mu_0(T) + \mu_R(\tau,\delta) \tag{4}$$

where $\mu_0(T)$ is the viscosity of the dilute gas, and $\mu_R(\tau,\delta)$ is the residual part.

$$\lambda(\rho,T) = \lambda_0(T) + \lambda_R(\tau,\delta) + \lambda_c(\tau,\delta) \tag{5}$$

where $\lambda_0(T)$ is the thermal conductivity of the dilute gas, $\lambda_R(\tau,\delta)$ is the residual part, and $\lambda_c(\tau,\delta)$ is the critical enhancement of thermal conductivity.

*The computational method*

The pressure-based solver of the Ansys Fluent was employed to simulate the flow field of the LNJ. By using this solver, the flow and heat transfer equations can be solved in a coupled manner. Before the convergence of flow field was checked, the nitrogen properties were evaluated and updated according to the pressure and temperature on each compute node. At the fluid–solid interfaces, the conjugate heat transfer is used to calculate the heat transfer between the fluid and solid [10] , e.g.,

$$T_f\big|_{\text{wall}} = T_s\big|_{\text{wall}}, \quad \lambda_f \frac{\partial T_f}{\partial n}\Big|_{\text{wall}} = \lambda_s \frac{\partial T_s}{\partial n}\Big|_{\text{wall}} \tag{6}$$

where $T_f$ is the fluid temperature, $T_s$ is the solid temperature, $\lambda_f$ is the fluid thermal conductivity, $\lambda_s$ is the solid thermal conductivity, and $n$ is the common normal direction

of the interface. Moreover, in the model, the gravity, density, isobaric heat capability, and thermal conductivity are 9.81, 2500,760 and 2.5 , respectively.

**Simulation results and analysis**

To acquire the LNJ flow field, a simulation was performed by using the following parameters: inlet pressure of 40 MPa, outlet pressure of 20 MPa, initial temperature of 300 K, injection temperature of 100 K, and nozzle outlet diameter of 6 mm. Before simulation, the fluid part was the nitrogen gas. The initial temperature of the solid part was also set as 300 K.

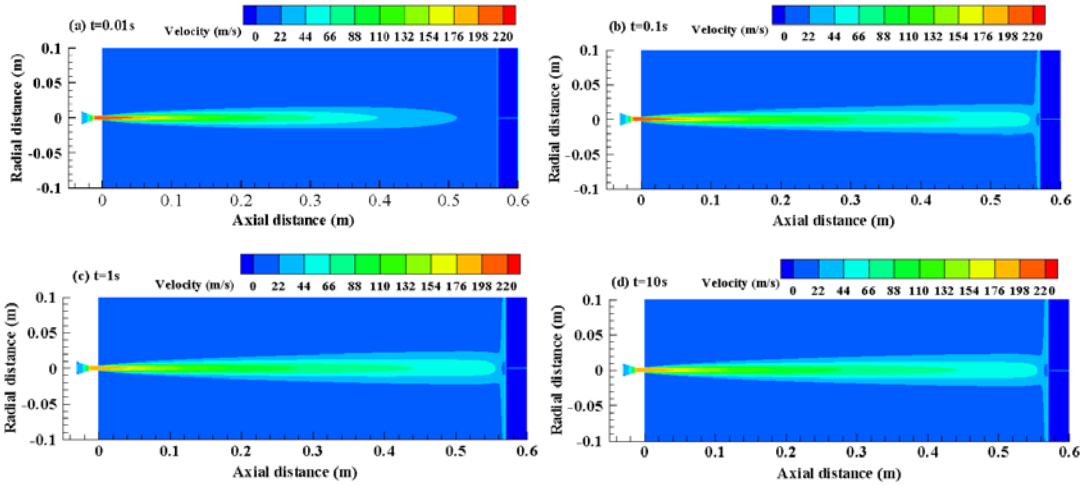


Fig. 2. The velocity fields of the LNJ at different times

*The velocity distributions*

As shown in Fig. 2, the velocity near nozzle was homogenous. As the jet developed along the axial direction, it continuously drew the surrounding fluid. Consequently, the jet flow region became increasingly wider while the jet velocity became progressively smaller. The boundary, where the velocity is equal to zero, is defined as the outer boundary (or velocity boundary). The LNJ also has obvious velocity boundary and potential core region. Moreover, the velocity remained unchanged in the potential core region. Fig. 3 shows the velocity distributions on eight different cross sections.

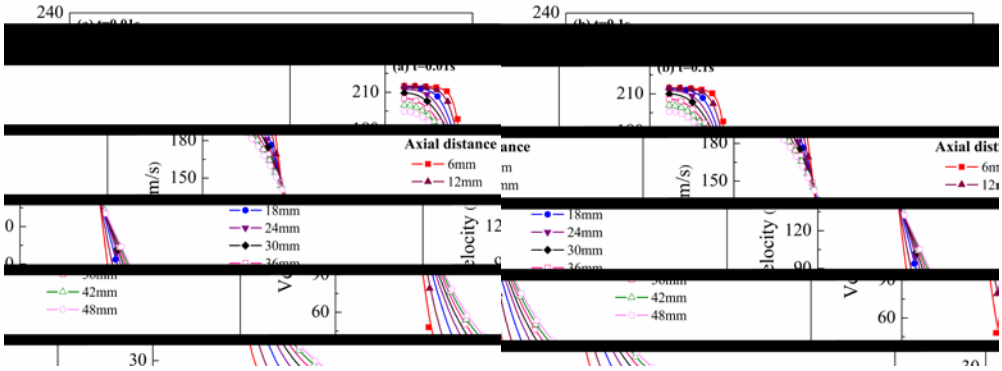

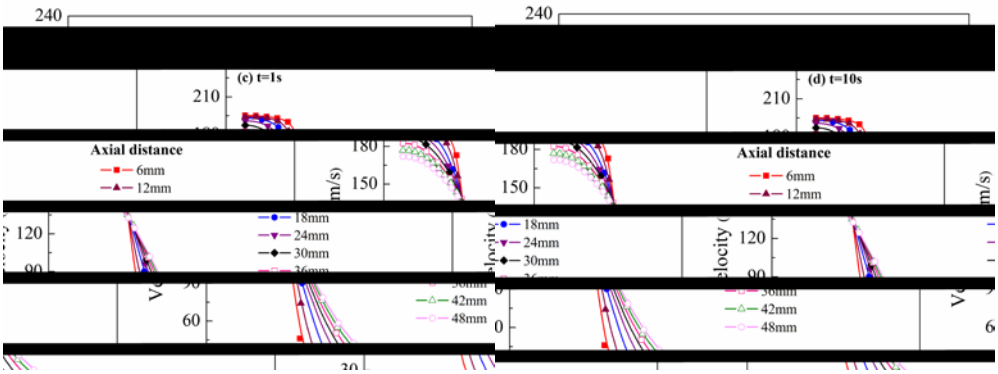


Fig. 3. Velocity distributions for different cross sections of LNJ at different times

*The temperature distributions*

Fig. 4 shows the jet temperature distributions along the axis at different times. The jet temperature increased with the growth of the axial distance because the jet continuously exchanged the mass and heat with the surrounding fluid along the axial direction. Consequently, the jet temperature gradually increased while the temperature of the surrounding fluid decreased. At 0.01 s and 0.1 s, the minimum temperature of the jet was higher than the nitrogen critical temperature (126.19 K) in the external region of the nozzle. It is indicated that LNJ could not be induced before 0.1 s due to the insufficient liquid nitrogen entering the flow domain. At 1 s, the jet temperature at the nozzle outlet became less than 126.19 K in the generation of the LNJ. According to the jet temperature distributions, the jet flow field can be divided into the LNJ and non-LNJ regions. The boundary between two regions was defined as the LNJ boundary.

Fig. 5 shows the temperature distributions of the different cross sections at the different times. With the growth of the radial distance, the temperature increased and finally was equal to the initial value. As the axial distance of the cross section increased, the heat transfer region, where the temperature was lower than the initial value, was also expanded. Owing to the heating effect of the surrounding fluid, the LNJ region is narrowed along the axial direction.

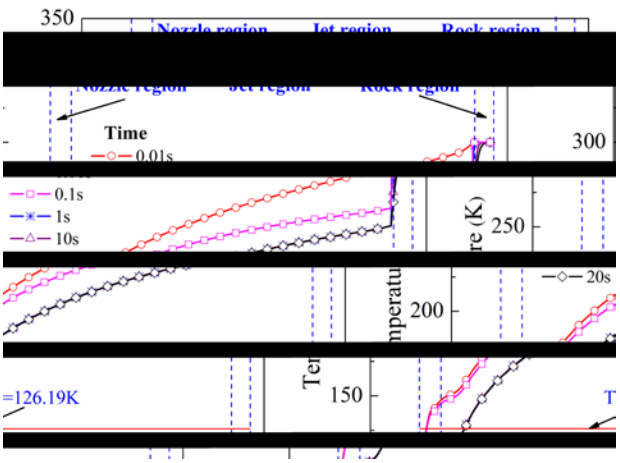


Fig. 4. The temperature distributions of the LNJ along the axis at the different times

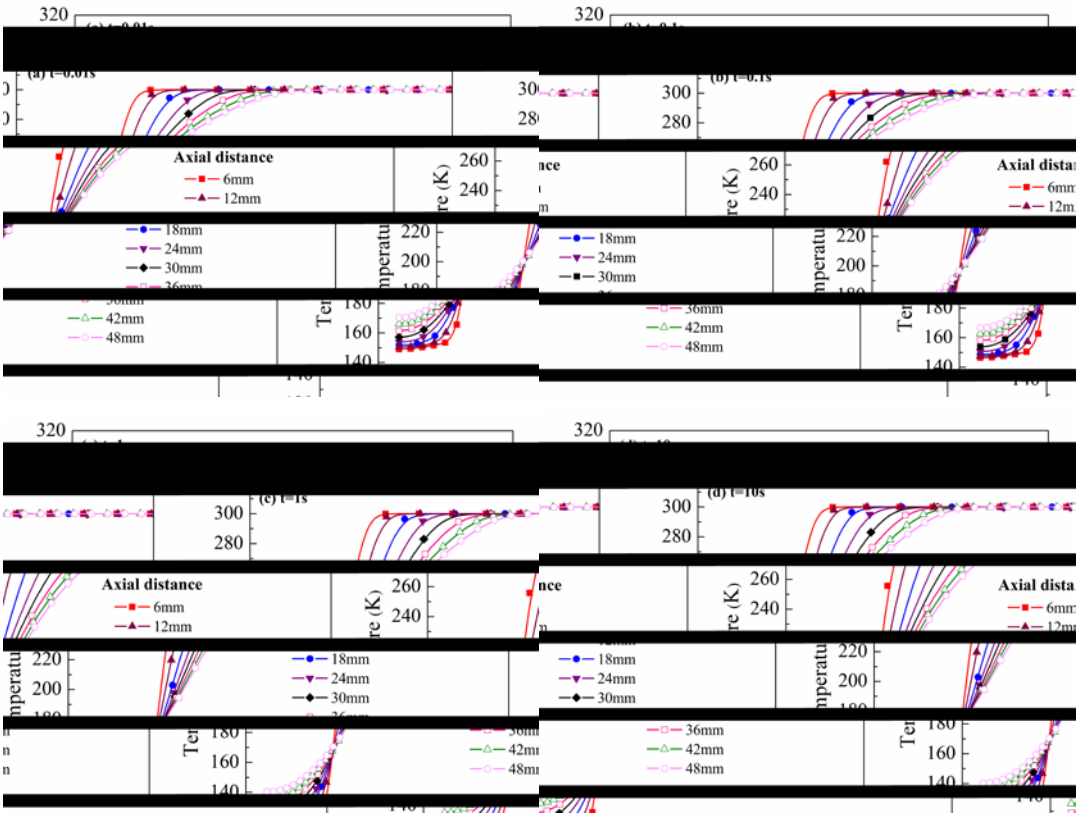


Fig. 5. The temperature distributions on the different cross sections of the LNJ at the different times

**Analysis of the flow field structure for the LNJ**

Based on the simulation results, the temperature boundary, velocity boundary, potential core boundary, and LNJ boundary were observed in Fig. 6. The line "CD" represented the velocity boundary (i.e., outer boundary), and the line "EG" denoted the potential core boundary (i.e., inner boundary). Given that the flow field was axisymmetric and the horizontal coordinate was the axis boundary condition, the distance from these boundaries to the axis was equal to the half width of the corresponding region. The width of line "AB," which depicted temperature boundary, was obviously greater than the velocity boundary. The width of the temperature boundary also increased linearly with the axial distance. Line "EF" was the LNJ boundary, within which the jet was in the liquid state. Unlike the potential core boundary, the width of the LNJ boundary decreased nonlinearly with the axial distance. Moreover, both the length and width of the LNJ region were larger than the potential core region. For example, at the axial distance of 12 mm, the width of the LNJ region was 72.54% higher than that of the potential core region. In addition, the length of the former was almost 1.8 times that of the latter.

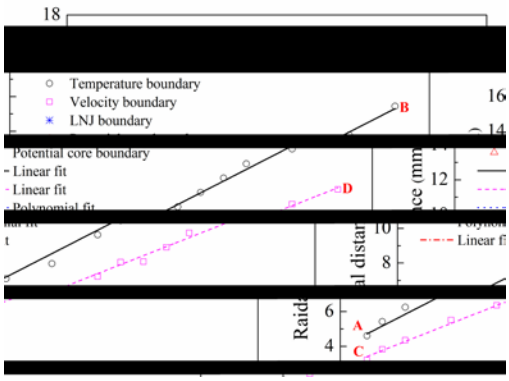


Fig. 6. Flow field structure analysis of LNJ (t=10 s)

## Conclusions

In our work, the LNJ exhibited an obvious velocity boundary and potential core region. This result indicated that high-speed jet could be efficiently produced as the high-pressure liquid nitrogen flowed through the nozzle. Besides the velocity boundary, the LNJ flow field also has a clear temperature boundary, on which the temperature is equal to the initial value. Within the temperature boundary, the jet flow field could be divided into the LNJ and non-LNJ regions. The velocity and temperature boundaries of the LNJ flow field are expanded with the growth of the axial distance. The width of the temperature boundary was greater than that of the velocity boundary, and the width and length of the LNJ region is larger than the potential core region.

## Acknowledgments

This work was financially supported by the National Natural Science Foundation of China (Grant No. 51604263), the Natural Science Foundation of Jiangsu Province (Grant No. BK20160252), and the State Key Research Development Program of China (Grant No. 2016YFC0600705).

## Nomenclature

$a$ - Helmholtz energy, [kJ/kg]

$C_p$ - Isobaric heat capacity, [J/ (kg·K)]

$p$ - Pressure [kPa]

$R$ - Gas constant, [kJ/ (kg·K)]

$T$ - Temperature, [K]

$T_c$ - Critical temperature, [K]

$\rho$ - Density, [kg/m$^3$]

$\rho_c$ - Critical density, [kg/m$^3$]

$\mu$ - Viscosity of nitrogen, Pa·s

$\lambda$ - Thermal conductivity, [W/ (m·K)]

$\mu_0$ = Viscosity of the dilute gas, [Pa·s]

$\mu_R$ - Residual part of viscosity, Pa·s

$\lambda_0$ - Thermal conductivity of the dilute gas, [W/ (m·K)]

$\lambda_R$ - Residual part of thermal conductivity, [W/( m·K)]

$\lambda_c$ - Critical enhancement of thermal conductivity, [W/( m·K)]

**References**


[1] Li, G., *et al.*, Research and applications of novel jet techniques in well drilling, completion and fracturing, *Science Foundation in China*, 22(2014), 2, pp. 68-80.

[2] Lai F., *et al.*, Impact of water blocking in fractures on the performance of hydraulically fractured horizontal wells in tight gas reservoir, *Journal of Petroleum Science and Engineering*, 156(2017), pp. 134-141.

[3] Zhang R., *et al.*, Environmentally friendly hydraulic fracturing and water-free fracturing technologies, *International Journal of Oil Gas & Coal Technology*, 17(2018), 4, pp. 375-390.

[4] Boudet H., *et al.*, "Fracking" controversy and communication: Using national survey data to understand public perceptions of hydraulic fracturing. *Energy Policy*, 65(2014), pp. 57-67.

[5] Cai C., *et al.*, Particle velocity distributions of abrasive liquid nitrogen jet and parametric sensitivity analysis. *Journal of Natural Gas Science and Engineering*, 27(2015), Part 3, pp. 1657-1666.

[6] Wu X., *et al.*, Investigation on the damage of high-temperature shale subjected to liquid nitrogen cooling. *Journal of Natural Gas Science and Engineering*, 57(2018), pp. 284-294.

[7] Cai C., *et al.*, Numerical simulation on the flow field characteristics and impact capability of liquid nitrogen jet. *Energy Exploration & Exploitation*, 36(2018), 5, pp. 989-1005.

[8] Wu X., *et al.*, Experiment on coal breaking with cryogenic nitrogen jet, *Journal of Petroleum Science and Engineering*, 169(2018), pp. 405-415.

[9] Gao F., *et al.*, Experimental research on rock fracture failure characteristics under liquid nitrogen cooling conditions, *Results in Physics*, 9(2018), pp. 252-262.

[10] Cai C., *et al.*, Downhole transient flow field and heat transfer characteristics during drilling with liquid nitrogen jet, *Journal of Energy Resources Technology-Transactions of The ASME*, 140(2018), 12, pp. 122902.

[11] Span R.., *et al.*, A reference equation of state for the thermodynamic properties of nitrogen for temperatures from 63.151 to 1000 K and pressures to 2200 MPa, *Journal of Physical and Chemical Reference Data*, 29(2000), 6, pp. 1361-1433.

[12] Lemmon E.W., *et al.*, Viscosity and thermal conductivity equations for nitrogen, oxygen, argon, and air, *International Journal of Thermophysics*, 25(2004), 1, pp. 21-69.



Paper submitted: May 11, 2018
Paper revised: June 1, 2018
Paper accepted: August 10, 2018